

STITCHER: Real-Time Trajectory Planning with Motion Primitive Search

Helene J. Levy and Brett T. Lopez

Abstract—Autonomous high-speed navigation through large, complex environments requires real-time generation of agile trajectories that are dynamically feasible, collision-free, and satisfy state or actuator constraints. Most modern trajectory planning techniques rely on numerical optimization because high-quality, expressive trajectories that satisfy various constraints can be systematically computed. However, meeting computation time constraints and the potential for numerical instabilities can limit the use of optimization-based planners in safety-critical scenarios. This work presents an optimization-free planning framework that stitches short trajectory segments together with graph search to compute long range, expressive, and near-optimal trajectories in real-time. Our STITCHER algorithm is shown to outperform modern optimization-based planners through our innovative planning architecture and several algorithmic developments that make real-time planning possible. Extensive simulation testing is conducted to analyze the algorithmic components that make up STITCHER, and a thorough comparison with two state-of-the-art optimization planners is performed. It is shown STITCHER can generate trajectories through complex environments over long distances (tens of meters) with low computation times (milliseconds).

I. INTRODUCTION

Planning collision-free and dynamically feasible trajectories through complex environments in real-time is a necessary capability for many autonomous systems. Trajectory planning has received considerable attention from the research community as a result, but achieving the reliability and computational efficiency required for real-world, safety-critical applications remains a challenge. In particular, few methods have guarantees in terms of trajectory optimality and time/memory complexity without sacrificing trajectory expressiveness, length, or computation time. Our proposed approach addresses this gap by combining optimal control theory with graph search to generate near-optimal trajectories over long distances in real-time without online optimization.

Optimization-based trajectory planning has emerged as the primary framework for autonomous systems that must navigate complex environments. This is because expressive trajectories can be naturally generated from the continuous nature of the solution space inherent to optimization problems. While approaches can be characterized based on several factors, most can be broadly classified by their use of continuous or integer variables. Continuous variable methods employ gradient descent to jointly optimize over the coefficients of basis functions (typically polynomials) and waypoint arrival times while imposing obstacle and state

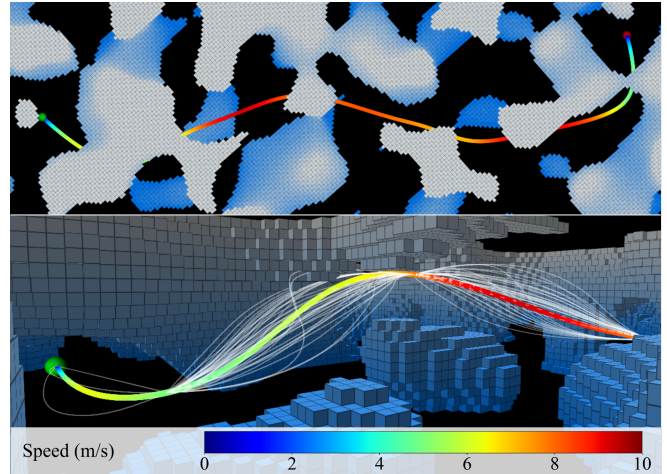


Fig. 1: A trajectory (colored based on speed) generated by our proposed algorithm called STITCHER through a perlin noise environment. STITCHER searches over candidates motion primitives (white) to find a safe trajectory in real-time with time and memory complexity guarantees.

constraints [1]–[6]. Integer variable methods require the free space of the environment be represented as the union of convex sets (continuous variable methods have also used this representation, e.g., [5], [6]) and solve a mixed-integer program for a collision-free trajectory [7]–[10]. Despite continued innovations, fundamentally these methods lack time complexity bounds that can be known *a priori*, and the approaches that rely on integer programming often scale very poorly with trajectory length.

A computationally efficient alternative to optimization-based trajectory planning is the use of so-called motion primitives: a library of short length/duration trajectories that can be efficiently computed and evaluated [11]–[14]. To effectively use motion primitives, a planner must operate in a receding horizon fashion, i.e., continuously replan, because motion primitives are of short length/duration. This can introduce several performance issues, e.g., myopic behavior or unexpressive trajectories, that are exacerbated in large, complex environments. Subsequent work has attempted to pose the problem as a graph search with nodes and edges being desired states (position, velocity, etc.) and motion primitives connecting neighboring nodes, respectively [15]–[18]. While this allows the creation of trajectories that cover long distances, the search times can be extremely high (seconds) because of the size of the graph and the difficulties of constructing an informative admissible search heuristic.

The main contribution of this work is a new trajectory planning algorithm called STITCHER that is capable of real-time motion primitive search over long distances through

Authors are with the VECTR Laboratory, University of California, Los Angeles, Los Angeles, CA, USA. {hjlevy, btlopez}@ucla.edu

complex environments. STITCHER utilizes an innovative three-stage planning architecture to generate smooth and expressive trajectories by *stitching* motion primitives together through graph search. First, a sequence of waypoints is constructed by finding a collision-free geometric path through the environment. Second, a velocity graph is created with nodes being a position and velocity pair where the positions correspond to those of the waypoints and the velocities are from a pre-defined finite set of candidate speeds and directions. Edges in the graph are solutions to the minimum-time input-constrained optimal control problem for a double integrator with boundary conditions being neighboring nodes in the graph. Critically, the cost-to-go from each node in the graph to the goal node is computed using the Bellman equation and saved for the next planning stage. Lastly, a graph search over motion primitives that are solutions to an optimal control problem is performed using A* where the heuristic is the cost-to-go computed in previous stage with the minimum-time double integrator. We prove the velocity and motion primitive graphs are finite and the proposed heuristic is admissible. These results are critical as they guarantee i) bounded time and memory complexity known *a priori* and ii) trajectory optimality with respect to the geometric path and sampled velocity set. Algorithmically, we develop an improved collision checking procedure based on [13] to leverage the known free space from previous trajectories, performing nearest neighbor searches on a point cloud map when necessary, thereby reducing computation time. STITCHER was extensively tested in two simulation environments to i) characterize various aspect of the algorithm and ii) evaluate its performance against two state-of-the-art optimization-based planners [5], [9] capable of running in real-time. STITCHER is shown to generate high-quality trajectories over long distances (over 50 m) with computation times in the milliseconds, and consistently outperforms the state-of-the-art in computation time.

II. RELATED WORKS

Optimization-based trajectory planners can be categorized using several criteria, but the clearest delineation is whether the method uses continuous or integer variables. For methods that use only continuous variables, the work by [2] reformulated [1] to jointly optimize over polynomial endpoint derivatives and arrival times for a trajectory passing through waypoints. Collisions were handled by adding intermediate waypoints and redoing the trajectory optimization if the original trajectory collided with the environment. Oleynikova et al. [3] represented obstacles using an Euclidean Signed Distance Field (ESDF) which was incorporated into a non-convex solver as a soft constraint. Zhou et al. [4] used a similar penalty-based method but introduced a topological path search to escape local minima. An alternative approach is to decompose free-space into convex polyhedra [7], [19] which can be easily incorporated as constraints in an optimization. The methods in [5], [6] treat these constraints as soft while efficiently optimizing over polynomial trajectory segments that must pass near waypoints. One can also use the

free-space polyhedra to formulate a mixed-integer program [8]–[10] to bypass the nonconvexity introduced by having unknown waypoint arrival times, but at the expense of poor scalability with trajectory length and number of polyhedra.

Motion primitive planners have been proposed as an alternative to optimization-based planners to address computational complexity and numerical instability concerns. The underlying idea of motion primitive planners is to select trajectories online from a precomputed, finite library of trajectories. Initial work on motion primitives for quadrotors leveraged differential flatness and known solutions to specific optimal control problems to efficiently compute point-to-point trajectories in real-time [11], [20]. Later work employed motion primitives for receding horizon collision avoidance where primitives were efficiently generated online by sampling desired final states, and selected at each planning step based on safety and trajectory cost [12]–[14], [21]. While computationally efficient, the behavior of these planners can be myopic, leading to suboptimal behavior in complex environments. One way to address nearsightedness is to extend traditional search-based algorithms, which typically use coarse discrete action sets, to using a lattice of motion primitives [15]–[17], [22], [23]. The main issue with search-based motion primitive planners is the search space can become untractable, and with the non-triviality of constructing an admissible search heuristic, search times are not suitable for real-time applications. Recently, [18], [24] proposed an efficient minimum-time motion primitive search in velocity space using a double integrator model restricted to pass through a set of waypoints. The search can be done in real-time but the resulting bang-bang acceleration profile is dynamically infeasible for quadrotors, leading to poor tracking performance. An additional smoothing step, e.g., model predictive contouring control, is required to achieve sufficient trajectory smoothness [24].

III. PROBLEM FORMULATION

This work is concerned with solving the following trajectory planning problem

$$\begin{aligned}
 \min_{\mathbf{u} \in \mathcal{U}} \quad & J = r(T) + \int_0^T q(\mathbf{x}, \mathbf{u}) dt \\
 \text{s.t.} \quad & \dot{\mathbf{x}} = A\mathbf{x} + B\mathbf{u} \\
 & \mathbf{x} \in \mathcal{X}_s, \mathbf{x} \notin \mathcal{X}_{obst}, \mathbf{u} \in \mathcal{U} \\
 & \mathbf{x}(0) = \mathbf{x}_0, \mathbf{x}(T) = \mathbf{x}_d,
 \end{aligned} \tag{1}$$

where $\mathbf{x} \in \mathbb{R}^n$ is the state that must satisfy state \mathcal{X}_s and obstacle (collision) \mathcal{X}_{obst} constraints, $\mathbf{u} \in \mathbb{R}^m$ is the control input that must satisfy actuator constraints \mathcal{U} , $A \in \mathbb{R}^{n \times n}$ and $B \in \mathbb{R}^{n \times m}$ govern the system's dynamics, and $r : \mathbb{R}_+ \rightarrow \mathbb{R}_+$ and $q : \mathbb{R}^n \times \mathbb{R}^m \rightarrow \mathbb{R}_+$ are the terminal and stage cost, respectively. The goal is to find an optimal final time T^* and feasible optimal state trajectory $\mathbf{x}^*(t)$ with a corresponding control input sequence $\mathbf{u}^*(t)$ for $t \in [0, T^*]$ that steers the system from an initial state \mathbf{x}_0 to a desired final state \mathbf{x}_d that minimizes the cost functional J . While the dynamics are linear in (1), many nonlinear systems can be placed into

the linear control affine form if they are differentially flat, e.g., VTOL vehicles like quadrotors, capturing a large class of systems of interest. In many cases, the state vector can be $\mathbf{x} = (\mathbf{r}, \mathbf{v}, \mathbf{a}, \dots, \mathbf{r}^{(p-1)})^\top$ and control input $\mathbf{u} = \mathbf{r}^{(p)}$ where $\mathbf{r} = (x, y, z)^\top$ is the vehicle's position coordinates.

A. Background: Motion Primitives

We define motion primitives to be closed-form solution to an optimal control problem. This work will focus on three specific optimal control problems, namely the minimum-time problem for a double integrator, the minimum-time problem for a triple integrator, and the linear quadratic minimum-time problem for a triple integrator. We will briefly review each optimal control problem and the structure of its solution. It is assumed all state constraints can be decoupled allowing the solution to be computed on per axis basis.

Minimum-Time Double Integrator: For an initial $(\mathbf{r}_0, \mathbf{v}_0)$ and desired final $(\mathbf{r}_f, \mathbf{v}_f)$ state, the minimum-time input-constrained double integrator optimal control problem is

$$\begin{aligned} \min_{\mathbf{u}} \quad & J = T \\ \text{s.t.} \quad & \ddot{\mathbf{r}} = \mathbf{u}, \quad \|\mathbf{u}\|_\infty \leq a_{max} \\ & \mathbf{r}(0) = \mathbf{r}_0, \quad \mathbf{v}(0) = \mathbf{v}_0 \\ & \mathbf{r}(T) = \mathbf{r}_f, \quad \mathbf{v}(T) = \mathbf{v}_f, \end{aligned} \quad (2)$$

where the final time T is free. From Pontryagin's minimum principle, the optimal control solution is known to have a bang-bang control profile along one of the position axes. The switching times can be computed by solving a quadratic equation. It is required each coordinate axis trajectory all have the same execution time, so the limiting minimum-time horizon is $T^* = \max\{T_x, T_y, T_z\}$. The limiting minimum-time horizon T^* , is then applied as a known variable for the non-limiting axes. This allows one to then solve a quadratic equation for a new bound $\check{a} \leq a_{max}$ on the control input.

Linear Quadratic Minimum-Time Triple Integrator: The linear quadratic minimum-time (LQMT) triple integrator optimal control problem takes the form

$$\begin{aligned} \min_{T, \mathbf{u}} \quad & J = \rho T + \int_0^T \|\mathbf{u}\|^2 dt \\ \text{s.t.} \quad & \mathbf{r}^{(3)} = \mathbf{u} \\ & \mathbf{r}(0) = \mathbf{r}_0, \quad \mathbf{v}(0) = \mathbf{v}_0, \quad \mathbf{a}(0) = \mathbf{a}_0 \\ & \mathbf{r}(T) = \mathbf{r}_f, \quad \mathbf{v}(T) = \mathbf{v}_f, \quad \mathbf{a}(T) \text{ free,} \end{aligned} \quad (3)$$

where $\rho > 1$ penalizes the final time and the final time T and final acceleration \mathbf{a}_f are free. The optimal trajectory is simply a fifth degree polynomial in time so the cost functional can be expressed analytically in terms of T and the known boundary conditions. The final time can be found efficiently using a root-finding algorithm such as a bisection search. Velocity and acceleration constraints are omitted from (3) as it is more efficient to prune solutions once the final time is known, as discussed in Section IV-D.

Minimum-Time Triple Integrator: The constrained

minimum-time triple integrator optimal control problem is

$$\begin{aligned} \min_{\mathbf{u}} \quad & J = T \\ \text{s.t.} \quad & \mathbf{r}^{(3)} = \mathbf{u}, \quad \|\mathbf{u}\|_\infty \leq j_{max} \\ & \|\mathbf{v}\|_\infty \leq v_{max}, \quad \|\mathbf{a}\|_\infty \leq a_{max} \\ & \mathbf{r}(0) = \mathbf{r}_0, \quad \mathbf{v}(0) = \mathbf{v}_0, \quad \mathbf{a}(0) = \mathbf{a}_0 \\ & \mathbf{r}(T) = \mathbf{r}_f, \quad \mathbf{v}(T) = \mathbf{v}_f, \quad \mathbf{a}(T) = \mathbf{a}_f, \end{aligned} \quad (4)$$

where T is free. From Pontryagin's minimum principle, the optimal control input can take several forms that involve various sequences of offs and bangs with up to seven switch times [25]. Computing the switching times is thus more involved, and in some cases requires a root-finding algorithm like Newton's method. We utilize the efficient implementation of Berscheid *et al.* [25] to generate solutions for this motion primitive class, in addition to their method for finding the limiting time horizon between the three axes.

IV. METHODOLOGY

STITCHER, detailed in Algorithm 1, generates a full-state trajectory by *stitching* collision-free, dynamically feasible trajectory segments together through graph search. At its core, STITCHER searches over closed-form solutions, i.e., motion primitives, to optimal control problems of the form discussed previously. These solutions essentially serve as a basis set for the solution space to (1). To achieve real-time performance, STITCHER utilizes a three step planning process where the final motion primitive search is guided by two other planners run sequentially that use low-dimensional models (see Fig. 2). In Stage 1 (left), a forward A* search is performed to produce a sparse geometric path, i.e., waypoints, in the free space of the environment (line 3); this is standard in many planning frameworks. In Stage 2 (middle), nodes representing sampled velocities at the waypoints are formed into a velocity graph where dynamic programming is used to compute the minimum time path from each node to the desired final state using an input-constrained double integrator model (lines 4-5). This step is critical for constructing an admissible heuristic to guide the full motion primitive search, and is one of the key innovations that enables real-time performance. It is important to note the optimal "path" in velocity space is never used; computing the cost-to-go is the primary objective as it serves as an admissible heuristic for motion primitive search as shown in Section V-B. In Stage 3 (right), a forward A* search is performed over motion primitives using a higher-order dynamical model and the cost-to-go from Stage 2 as an admissible heuristic. At this stage, position and all higher-order derivatives are considered yielding a full state trajectory that can be tracked by the system (lines 6-21). The remainder of this section expands upon each component of STITCHER.

A. Stage 1: Forward Geometric Path Search

STITCHER requires a sequence of waypoints that essentially guides the motion primitive search by limiting the size of the search space. This can be done by generating a collision-free geometric path (see Fig. 2 left) through the

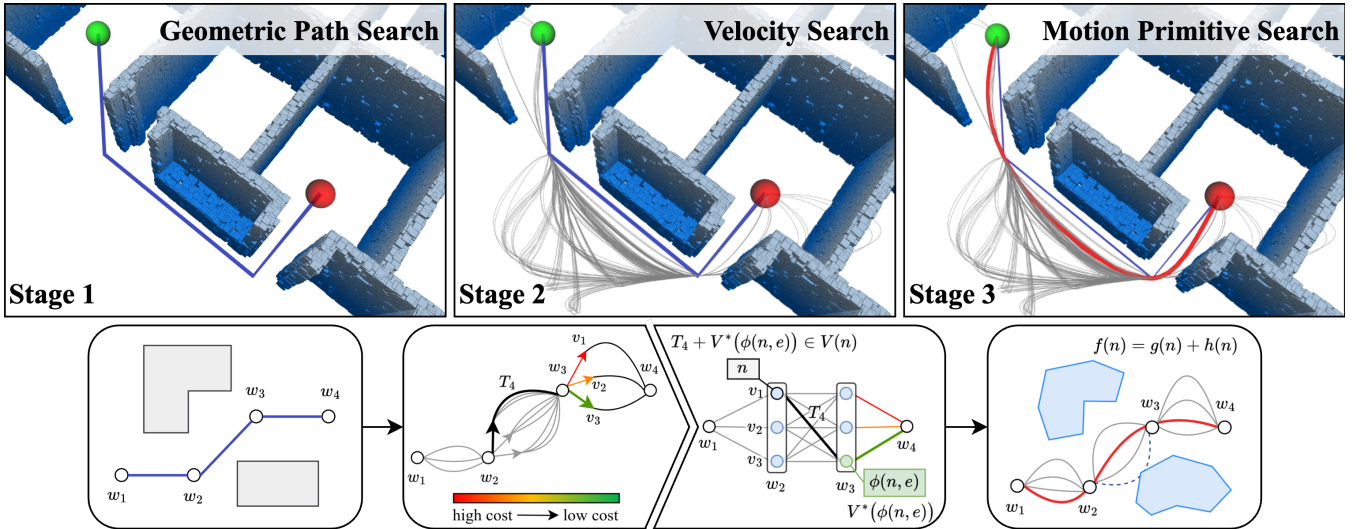


Fig. 2: System architecture describing the three planning stages. In Stage 1, a sparse geometric path is found via an A* search through the voxelized environment. In Stage 2, a velocity state is then introduced at each waypoint and dynamic programming is used to recursively solve for the cost-to-go at each node. In Stage 3, a full motion primitive search informed by the previous stages is performed, and checks for collisions to yield the final trajectory.

Algorithm 1: STITCHER Trajectory Planner

```

1 input:  $\mathcal{P} \leftarrow$  point cloud,  $n_s \leftarrow$  start,  $n_g \leftarrow$  goal;
2 output:  $s^*(t)$ ;
   // extract waypoints and path features
3  $\mathbf{w}, \mathbf{q}, \mathcal{H} \leftarrow$  getGeometricPath( $\mathcal{P}, n_s, n_g$ );
4  $\mathcal{G} \leftarrow$  buildVelocityGraph( $\mathbf{w}, \mathbf{q}, \mathcal{H}$ );
   // get heuristic from recursive cost-to-go
5  $h(n) \leftarrow$  dynamicProgramming( $\mathcal{G}, n_s, n_g$ );
6  $\mathcal{G}_{mp} \leftarrow$  buildFullStateGraph( $\mathcal{G}$ );
7 function planPath( $\mathcal{P}, \mathcal{G}_{mp}, n_s, n_g$ ):
8    $n_{curr} = n_s$ ;
9   while  $n_{curr} \neq n_g$  do
10     // get node with lowest cost  $g(n)+h(n)$ 
11      $n_{curr} = \text{OPEN.pop}()$ ;
12     if  $n_{curr} = n_g$  then
13       break;
14     end
15      $\mathcal{E}_{n_{curr}} \leftarrow$  getSuccessors( $n_{curr}, \mathcal{G}_{mp}$ );
16     for  $e$  in  $\mathcal{E}_{n_{curr}}$  do
17       // collision and state constraint check
18       pruneMotionPrimitive( $e, \mathcal{P}$ );
19        $\text{OPEN.insert}(\phi(n, e))$ ;
20     end
21 end
22  $s^*(t) \leftarrow$  getFinalMotionPrimitives( $n_{curr}, \text{CLOSED}$ );

```

environment with A* search or any other discrete graph search algorithm where the environment is represented as a 3D voxel grid where each grid cell contains occupancy information. Let the collision-free, geometric path generated by a discrete graph search algorithm be composed of points $\mathcal{O} = \{\mathbf{o}_1, \mathbf{o}_2, \dots, \mathbf{o}_H\}$ where $\mathbf{o}_i \in \mathbb{R}^3$. The set of points \mathcal{O} is further pruned to create a sparse set of waypoints $\mathcal{W} = \{\mathbf{w}_1, \mathbf{w}_2, \dots, \mathbf{w}_N\}$ where $N \leq H$ and $\mathbf{w}_i \in \mathbb{R}^3$. Sparsification is done by iterating through each point \mathbf{o}_i and directly drawing a straight line segment to the next valid point $\mathbf{o}_j \in \mathcal{O}$ until collision. The geometric path search is shown in line 3 of Algorithm 1.

B. State 2: Backward Velocity Search

The ordered waypoint set \mathcal{W} found in Stage 1 only provides a collision-free geometric path through the environment. In other words, velocity, acceleration, etc. required by tracking controllers is not specified. We propose creating a velocity graph (see Fig. 2 middle) where each node in the graph is defined by a position and velocity. The positions are restricted to waypoint locations and M velocities are sampled at each waypoint. More explicitly, for each waypoint $\mathbf{w}_i \in \mathcal{W}$, we sample a set of velocities $\mathcal{V} = \{\mathbf{v}_1, \dots, \mathbf{v}_M\}$, where \mathcal{V} is composed of candidate velocity magnitudes \mathcal{V}_m and directions \mathcal{V}_d . The choice of \mathcal{V}_m and \mathcal{V}_d can impact the STITCHER's performance in-terms of path optimality and computational complexity; this point will be discussed in more detail in Section VI.

With the ordered waypoint \mathcal{W} and sampled velocity \mathcal{V} sets, we create a velocity graph $\mathcal{G} = (\mathcal{N}, \mathcal{E})$, where node $n \in \mathcal{N}$ is a given position and sampled velocity, i.e., $n = (\mathbf{w}_i, \mathbf{v}_j)$ with $\mathbf{w}_i \in \mathcal{W}$ and $\mathbf{v}_j \in \mathcal{V}$, and edge $e \in \mathcal{E}$ is the *double integrator input-constrained minimum-time* motion primitive from (2) that connects neighboring nodes. Recall the solution to (2) is fully determined by having an initial and final position and velocity pair which is precisely how each node in \mathcal{N} is defined. At this stage, collisions and state constraints are not checked to prevent candidate trajectories from being prematurely eliminated.

We recursively compute and store the ranked list of cost-to-go's $V_d : \mathcal{N} \times \mathcal{E} \rightarrow \mathbb{R}_+$ for each node $n \in \mathcal{N}$ and all connecting edges $e \in \mathcal{E}_n$ of n where

$$V_d(n, e) = \ell(n, e) + V_d^*(\phi(n, e)) \quad \forall e \in \mathcal{E}_n, \quad (5)$$

with the optimal cost-to-go $V_d^*(n) = \min_{e \in \mathcal{E}_n} V_d(n, e)$, the cost of taking edge e from node n being $\ell(n, e)$, and the node reached by taking edge e being $\phi(n, e)$. The cost of taking an edge is $\ell(n, e) = T_d^*(n, e)$, where $T_d^*(n, e)$ is the minimum-time of the optimal trajectory connecting the states of node n to the states of $\phi(n, e)$. Equation (5) in

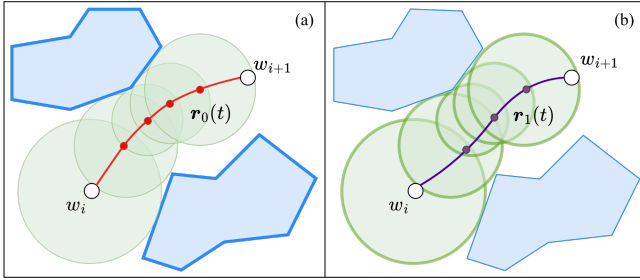


Fig. 3: Removing redundant collision checks. (a): Motion primitive $r_0(t)$ checks for collisions using [13]. (b): Sampled points of $r_1(t)$ are checked to lie within obstacle-free regions derived from $r_0(t)$ calculations.

conjunction with the min operator is the well-known Bellman equation that is guaranteed to return the optimal cost-to-go. In Section V-B we prove $V_d^*(n)$ for each node in a graph \mathcal{G} is an admissible heuristic for an A* search over a broad class of motion primitives. Building and searching the velocity graph are shown in lines 4-5 of Algorithm 1.

C. Stage 3: Forward Motion Primitive Search

The cost-to-go's computed in Stage 2 for the sampled velocities at each waypoint serve as an admissible heuristic (see Definition 1 for a precise definition) that guides an efficient forward A* search over motion primitives. The motion primitives can be generated using any chain of integrators model of order at least two so long as i) the initial and final position and velocity match those used to construct the velocity graph \mathcal{G} and ii) the limit on acceleration a_{max} is the same of that in (2). The motion primitive search graph is denoted as $\mathcal{G}_{mp} = (\mathcal{N}_{mp}, \mathcal{E}_{mp})$ where \mathcal{N}_{mp} is the set of nodes, each corresponding to a state vector, and \mathcal{E}_{mp} is the set of edges, each corresponding to a motion primitive that connecting neighboring nodes. A* search is used to meet real-time constraints where the search minimizes the cost $f(n) = g(n) + h(n)$ where $n \in \mathcal{N}_{mp}$ is the current node, $g : \mathcal{N}_{mp} \rightarrow \mathbb{R}_+$ is the cost from the start node n_s to node n , and $h : \mathcal{N}_{mp} \rightarrow \mathbb{R}_+$ is the estimated cost from the current node n to the goal node n_g . Using optimal control terminology, g is the cost accrued, i.e., the cost functional J , for a path from n_s to n whereas h is the estimated cost-to-go, i.e., the estimated value function V^* , from n to n_g . In this stage, collision and state constraints are checked for each candidate motion primitive to ensure safety. The methodology for both is discussed in Section IV-D. Each step of the motion primitive A* search is shown in lines 6-21 of Algorithm 1.

D. Pruning Infeasible & In-Collision Motion Primitives

STITCHER guarantees safety by pruning motion primitives from the final search that violate state constraints or are in collision. For state constraints, a motion primitive is sampled in time to verify constraints, e.g., $\|v\|_\infty \leq v_{max}$, $\|a\|_\infty \leq a_{max}$, etc., are satisfied. While creating a convex hull around polynomials is one method for enforcing state constraints as demonstrated in [17], this is often done out of necessity when doing optimization-based planning. Conversely, STITCHER has the freedom to use different

methods for enforcing state constraints. We chose discretization to avoid conservatively eliminating safe paths since the observed computation times of sampling were negligible.

An efficient collision checking strategy was devised by constructing a safe set of spheres resulting from a sampling-based collision checking approach developed in [13] (see Fig. 3). The core idea from [13] is that a trajectory can be intelligently sampled for collisions by estimating the next possible “time-of-collision” along the trajectory by combining obstacle proximity and the vehicle’s maximum speed. Leveraging this idea, further computation time savings can be achieved by storing and reusing nearest neighbor queries. Algorithm 2 details our strategy which takes in a k -d tree data structure filled with points from a point cloud \mathcal{P} of the environment. For the first candidate motion primitive connecting two successive waypoints, we use the strategy from [13] to intelligently sample for collisions while also storing the resulting set of safe, obstacle-free spheres \mathcal{S} , defined by center and radius vectors, c and \mathbf{R} (line 4). For subsequent motion primitives between the same waypoint pair, a nearest neighbor query is only done if the primitive is expected to leave the initial set of obstacle-free spheres. For a point found to be within a certain sphere (lines 14-17), the next possible “time-of-collision” is when the trajectory intersects the edge of the sphere, which can be estimated by assuming the trajectory is emanating radially from the center of the sphere at maximum velocity (line 18). The process is repeated until the final time horizon T is reached. Unlike spherical safety corridors, our safe set is only used as a means to avoid repeated calculation, and allows for on-the-fly addition of collision-free spheres. In other words, our approach does not restrict solutions to remain within convex sets centered along the geometric path. STITCHER thus has the flexibility to create and check candidate trajectories without being restricted to pre-defined safety spheres.

E. Motion Primitive Search Graph with Triple Integrator

In many applications, a triple integrator model is sufficient for generating motion primitives because the resulting trajectory is smooth enough for most vehicles, e.g., quadrotors, to track as discontinuities in jerk do not severely degrade tracking. However, one may require a free or fixed terminal acceleration depending on the optimal control problem used to generate the motion primitive. We have two separate formulations for the full state graph \mathcal{G}_{mp} for each case.

If the acceleration at each node, i.e., the final acceleration, a_f , is free, then the motion primitive search graph \mathcal{G}_{mp} is identical in size to the velocity graph \mathcal{G} (graph size detailed in Section V-A) since the number of nodes and edges are respectively equal. This formulation offers an advantage in terms of computational efficiency, as a full state trajectory is generated while the graph size is restricted by only the number of sampled velocities. Free terminal acceleration is a natural choice for the LQMT optimal control problem (3). Conversely, if the acceleration at each node a_f is specified, then the velocity graph \mathcal{G} must be augmented with a set of accelerations \mathcal{A} when creating the motion primitive

Algorithm 2: Collision Check

```

1 input:  $\mathcal{T} \leftarrow k$ -d tree,  $\mathbf{r}(t) \leftarrow$  motion primitive,
2 output: bool collision
3 if  $S = \emptyset$  then
4     // initial collision check using k-d tree
5     collision,  $S \leftarrow$  collisionCheckMap( $\mathbf{r}(t)$ ,  $\mathcal{T}$ );
6     return collision
7 end
8  $\tau \leftarrow 0$ ;
9  $d_{min} \leftarrow \infty$ ;
10 while  $\tau \leq T$  do
11      $\mathbf{d} \leftarrow$  calcDistToSphereCenters( $\mathbf{c}$ ,  $\mathbf{r}(\tau)$ )
12     for  $i = 1$  to  $|\mathcal{S}|$  do
13         if  $d_i < R_i$  &  $d_i \leq d_{min}$  then
14              $d_{min} \leftarrow d_i$ ;
15              $k \leftarrow i$ ;
16         end
17     end
18     if  $d_{min} < \infty$  then
19         // update sample time
20          $\tau \leftarrow \tau + (R_k - d_k)/v_{max}$ ;
21     else
22         // point outside spheres, use k-d tree
23         collision,  $S \leftarrow$  collisionCheckMap( $\mathbf{r}(t)$ ,  $\mathcal{T}$ );
24     end
25 end
26 return collision

```

search graph \mathcal{G}_{mp} . For a node n of graph \mathcal{G} , we define the incoming and outgoing edges as $\bar{\mathcal{E}}_n$ and \mathcal{E}_n , respectively. The set of possible accelerations $\mathcal{A}(n)$ derived from node n are $\mathcal{A}(n) = \{\bar{\mathbf{a}} \in \bar{\mathcal{E}}_n, \mathbf{e} \in \mathcal{E}_n \mid \bar{\mathbf{a}}(n) = (\mathbf{a}_{\bar{\mathbf{e}}}(T) + \mathbf{a}_{\mathbf{e}}(0))/2\}$ where $\mathbf{a}_{\bar{\mathbf{e}}}(T)$ is the terminal acceleration of the motion primitive represented by edge $\bar{\mathbf{e}}$, and $\mathbf{a}_{\mathbf{e}}(0)$ is the initial acceleration of the motion primitive represented by edge \mathbf{e} . Hence, given the velocity graph \mathcal{G} , $|\mathcal{A}(n)|$ new nodes must be created in the motion primitive graph \mathcal{G}_{mp} to incorporate an acceleration constraint. Fixed terminal acceleration is a natural choice for the minimum-time optimal control problems, but comes at the expense of having higher computation times because of the larger graph size.

V. THEORETICAL ANALYSIS

In this section we prove STITCHER has bounded time and memory complexity by showing the velocity and motion primitive graphs are finite. We also show STITCHER is complete and optimal by proving the heuristic used in the motion primitive search is admissible.

A. Velocity Graph Complexity

The following proposition proves the size of the velocity graph \mathcal{G} is finite and solely depends on the number of waypoints and sampled velocities; a property that also holds for the motion primitive graph \mathcal{G}_{mp} by extension. This result is critical as a finite graph yields *known time complexity* for the motion primitive search. In other words, an upper bound can be placed on how long it takes to generate a trajectory given known quantities. This is in contrast to optimization-based methods where the time complexity depends on the number of iterations required to converge—which cannot be

known *a priori*—so the time to compute a trajectory via optimization does not have an *a priori* bound.

Proposition 1. For N waypoints and M sampled velocities, the number of nodes $|\mathcal{N}|$ and edges $|\mathcal{E}|$ in graph \mathcal{G} is

$$|\mathcal{N}| = (N - 2)M + 2, \quad (6)$$

$$|\mathcal{E}| = (N - 3)M^2 + 2M \text{ for } N > 2. \quad (7)$$

Proof. Using Fig. 2 (middle), the start and goal nodes contribute 2 nodes to the graph \mathcal{G} . For intermediate waypoints, given M sampled velocities, there are M nodes per waypoint. As a result, $|\mathcal{N}| = (N - 2)M + 2$ which is (6). For each edge, we consider the transition to successive waypoints. Ignoring the trivial $N = 2$ case where $|\mathcal{E}| = 1$, there are M connections between the start node and next waypoint, which also has M nodes. The same applies for connecting waypoint w_{N-1} to the goal node, resulting in a total of $2M$ edges. For all other intermediate waypoint pairs, M nodes connect to M nodes at the next waypoint so there are M^2 edges. The total number of edges is then (7). \square

Corollary 1. The size of the motion primitive graph \mathcal{G}_{mp} using Linear Quadratic Minimum Time (LQMT) motion primitives with free terminal acceleration for a triple integrator is identical to the velocity graph \mathcal{G} .

Proof. The proof is immediate since the terminal acceleration is free so N and M are identical for both graphs. \square

Remark 1. Corollary 1 can be generalized to any motion primitive search graph where the primitives are solutions to an optimal control problem with the dynamics being a chain of integrators and all terminal state derivatives of second order or higher are free.

B. Admissible Heuristic for Motion Primitive Search

It is well known that heuristics can be used to expedite searching a graph by incentivizing exploring promising nodes. For example, in A* search, the next node explored is selected based on minimizing the cost $f(n) = g(n) + h(n)$, where g is the stage cost to get from the start node n_s to node n , and h is an estimate of the remaining cost to reach the goal node n_g . A* search is guaranteed to find an optimal solution so long as the heuristic function h is admissible (see Definition 1) [26]. Below, we prove the cost-to-go V_d^* for each node in the velocity graph \mathcal{G} calculated in Stage 2, i.e., the minimum-time to goal for a double integrator, is an admissible heuristic for an A* search over motion primitives of any higher-order chain of integrators.

Definition 1 ([26]). A function $h : \mathcal{N} \rightarrow \mathbb{R}$ is an admissible heuristic if for all $n \in \mathcal{N}$ then $h(n) \leq h^*(n)$, where h^* is the optimal cost from n to the goal node n_g .

Lemma 1. Consider the optimal control problem

$$\begin{aligned} \min_{T, \mathbf{u}} \quad & J = \rho T + \int_0^T q(\mathbf{r}, \mathbf{v}, \dots, \mathbf{u}) dt \\ \text{s.t.} \quad & \mathbf{r}^{(p)} = \mathbf{u}, \quad \|\mathbf{a}\|_\infty \leq a_{max} \\ & \mathbf{r}(0) = \mathbf{r}_0, \quad \mathbf{v}(0) = \mathbf{v}_0, \dots \\ & \mathbf{r}(T) = \mathbf{r}_f, \quad \mathbf{v}(T) = \mathbf{v}_f, \dots \end{aligned} \quad (8)$$

where q is a positive definite function, the system is at least second order ($p \geq 2$), and a_{max} is the same maximum acceleration as in (2). Further, let the initial and final position and velocities be identical to those of (2), with all other initial and final conditions being arbitrary. If V^* is the optimal cost-to-go from the initial conditions for (8) and T_d^* is the optimal final time for (2) then $V^* \geq \rho T_d^*$.

Proof. First, it is known that the optimal final time T_d^* for (2) is guaranteed to exist and be unique [27]. Consequently, for $p = 2$, the final time T for (8) and T_d^* for (2) will be identical if $q = 0$. When q is nonzero, it follows that $V^* \geq \rho T_d^*$ because the running cost is always non-negative. For any $p > 2$, a similar argument can be made based on the existence and uniqueness of T_d^* . Specifically, T for (8) must satisfy $T \geq T_d^*$ where equality can only be achieved if the acceleration profile for (8) matches the bang-bang solution to (2). However, this would require impulses in the optimal control input \mathbf{u}^* for (8) which is known to not be a characteristic of any solution to the general problem (8) [27]. Thus $V^* \geq \rho T_d^*$ for any $p \geq 2$, as desired. \square

Remark 2. Lemma 1 also holds when inequality constraints on the states and/or control in (8) are present.

The main result of this section can now be stated.

Theorem 1. The optimal cost-to-go for the minimum-time input-constrained double integrator optimal control problem (2) is an admissible heuristic for motion primitive search where the primitives are solutions to the optimal control problem of the form (8).

Proof. Let $\mathcal{G} = (\mathcal{N}, \mathcal{E})$ be a graph with nodes being sampled velocities at waypoints and edges being the time-optimal trajectories using an input-constrained double integrator. Further, let $\mathcal{G}_{mp} = (\mathcal{N}_{mp}, \mathcal{E}_{mp})$ be a graph with nodes being sampled velocities, accelerations, etc. at waypoints and edges being trajectories that are solutions to (8). Using the Bellman equation, the optimal cost-to-go $V_{mp}^*(n)$ for any $n \in \mathcal{N}_{mp}$ can be computed recursively. Using Lemma 1, $V_{mp}^*(n) \geq V_d^*(n')$ by induction where V_d^* is the optimal cost-to-go for the minimum-time input-constrained double integrator with $n' \in \mathcal{N}$. Recognizing $\mathcal{N} \subseteq \mathcal{N}_{mp}$, $V_d^*(n')$ can be rewritten as $V_d^*(n)$. Setting $h^*(n) = V_{mp}^*(n)$ and $h(n) = V_d^*(n)$, it can be concluded $h(n) \leq h^*(n)$. Therefore, by Definition 1, the optimal cost-to-go computed for \mathcal{G} is an admissible heuristic for the motion primitive search over \mathcal{G}_{mp} . \square

The importance of Theorem 1 follows from the well-known result that searching a graph with an admissible heuristic is *guaranteed* to return the optimal path through the

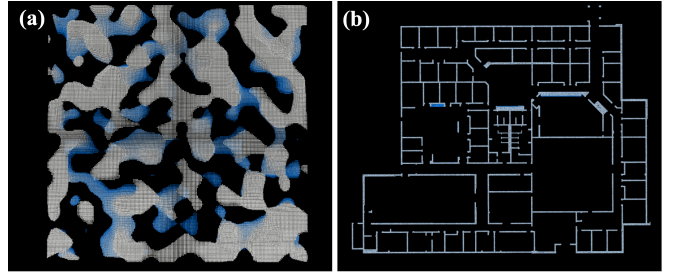


Fig. 4: Simulation test environments. (a): Perlin noise environment. (b): Willow Garage environment.

graph [26], and can significantly improve search efficiency because not every node in the graph has to be explored. The effectiveness of the proposed heuristic both in terms of path quality and search times is analyzed in Section VI.

VI. SIMULATION RESULTS

This section presents an analysis of STITCHER. First, we conduct a parameter sensitivity study to determine a suitable sampled velocity set (direction and speed) using a modified version of Dijkstra’s algorithm that has access to a dense set of velocities and no constraints on computation time. Second, we compare STITCHER’s performance as measured by computation and trajectory execution time to the aforementioned offline Dijkstra search. Both linear quadratic minimum time (LQMT) (3) and minimum-time (4) motion primitives were evaluated. Note the minimum-time triple integrator motion primitive study is to simply show STITCHER can use different primitive classes as the solution to (4) requires online optimization [25]. Third, we investigate the effectiveness of the heuristic proposed in Section V-B in reducing the number of edges generated by STITCHER. Fourth, we characterize the average computation time of the different components that make up STITCHER. Lastly, STITCHER is compared to two optimization-based modern planners [5], [9] capable of running in real-time.

Simulation experiments were run in a perlin noise environment and the Willow Garage environment, both with a volume of approximately $50 \times 50 \times 5$ m (see Fig. 4). Geometric paths with $N = 4, 6, 8$ waypoints were found for different start and end locations in each environment. For the perlin noise environment, the path lengths were 12.5 m, 30 m, and 55 m while the path lengths for Willow Garage were 20 m, 25 m, and 30 m for $N = 4, 6, 8$ waypoints, respectively. For all experiments, $v_{max} = 10$ m/s, $a_{max} = 10$ m/s², and $j_{max} = 60$ m/s³. A time penalty of $\rho = 1000$ was used for the LQMT motion primitives. All reported times are from tests conducted on an 11th generation Intel i7 laptop.

A. Offline Method for Generating Optimal Trajectories

Before presenting our analysis, we discuss the method for computing optimal trajectories used to evaluate STITCHER’s performance. Since STITCHER requires a sampled velocity set \mathcal{V} , we modified Dijkstra’s algorithm to search over a dense set of velocities and/or accelerations given a motion primitive class to generate a suitable comparison. Dijkstra is

a complete and optimal search algorithm where optimality is with respect to the set of actions, i.e., sampled states for our case [26], making it a suitable benchmark. Note that global optimality for the trajectory planning problem cannot be claimed though because only one waypoint path is considered from the onset. For the LQMT trajectories, a densely sampled search with 3611 terminal velocities at each waypoint was conducted. For the minimum-time trajectories, which require both a terminal velocity and acceleration, the densely sampled states were 197 velocities and 197 accelerations, resulting in a total of 38,809 states per waypoint. This search was used to bootstrap a finer local search to obtain an optimal solution. The Dijkstra search can only be run offline given the enormity of the search space, but, as will be shown next, STITCHER can generate near-optimal solutions in real-time. We will refer to the offline search method as *Dense Dijkstra* in the sequel.

B. Parameter Sensitivity Analysis: Sampled Velocity Set

STITCHER requires a discrete velocity set \mathcal{V} which is composed of a set of magnitudes and directions. As shown in Section IV-B, the size of the velocity graph scales quadratically with the number of sampled velocities so it is desirable to choose \mathcal{V} to be small without degrading path quality. We conducted two studies using LQMT motion primitives to determine i) the predominate sampled velocity directions used by Dense Dijkstra and ii) the trade-off between path cost and the number of sampled speeds.

1) *Sampled Direction*: To help inform the choice of the velocity direction set \mathcal{V}_d , we used Dense Dijkstra discussed above to statistically identify velocity directions commonly employed in a variety of test cases. Using Fig. 5 as a guide, we define angles with respect to the hyperplane \mathcal{H} with normal vector \hat{a} at the plane of symmetry between path segments connecting two waypoints. Table I shows the frequency of velocity directions chosen by Dense Dijkstra across all motion primitives for six different path length trials in the perlin noise and Willow Garage environment. The search was given velocity zeniths sampled in 10° increments in the range $[0^\circ, 180^\circ]$, and azimuth in the range $[-90^\circ, 90^\circ]$. The velocities chosen by Dense Dijkstra align with the normal vector \hat{a} of the hyperplane 80% of the time. From these results, sampling at the center and boundaries of a 20° cone centered around a given \hat{a} will yield a suitable set of velocity directions.

2) *Sampled Speed*: Using the identified velocity direction set \mathcal{V}_d from above, the performance of Dense Dijkstra was analyzed with different sampled speed set \mathcal{V}_m . Figure 6 shows the execution time (left) and planning times (right) for different sizes of the sampled speed set. The sampled speed sets with k elements, i.e., $|\mathcal{V}_m| = k$, were defined to have k elements evenly spaced in the interval $[0, v_{max}]$. The execution time increases as the sampled speed set becomes sparser, which is expected because the planner has fewer speed options to select from. However, the observed increase in execution time is at most 8% with the sparsest speed set tested. Critically, the minimal increase in execution time is

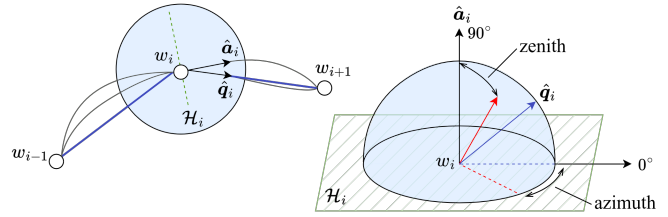


Fig. 5: Velocity directions sampled at waypoint w_i , where \hat{a}_i is normal to the separating hyperplane \mathcal{H}_i and \hat{q}_i is the heading toward w_{i+1} .

TABLE I: Frequency of Velocity Directions in Final Trajectory.

Zenith Angle	70°	80°	90°	100°	110°	
Frequency	0%	13%	79%	8%	0%	
Azimuth Angle	-50°	-20°	-10°	0°	10°	20°
Frequency	4%	4%	17%	42%	29%	4%

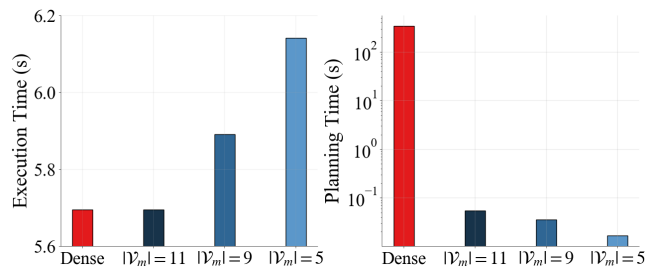


Fig. 6: Analysis of speed discretization on execution and planning time. As the discretization of our method is increased, we converge to the Dense Dijkstra solution. We use $\mathcal{V}_m = 5$ for our experiments as it achieves significant computational advantages while retaining suitable performance.

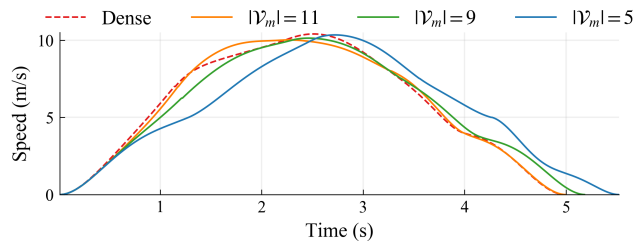


Fig. 7: Velocity profiles from varying speed discretizations in STITCHER. As the number of speed samples increases, STITCHER converges to the optimal solution.

accompanied by a significantly reduction in planning times: a speed up of four orders of magnitude with the sparsest sampled speed set tested was observed. Even though a sample speed set size of $|\mathcal{V}_m| = 11$ yields nearly equal execution times with the dense set, and a three orders of magnitude improvement in planning time, adequate performance can be achieved when $|\mathcal{V}_m| = 5$. Hence, we use the set $\mathcal{V}_m = \{0, 0.25 v_{max}, 0.5 v_{max}, 0.75 v_{max}, v_{max}\}$ for the remainder of our analysis. A representative speed profile for different sized speed sets is shown in Fig. 7.

C. Trajectory Optimality Characterization

The trajectories generated by STITCHER with the sampled velocity set \mathcal{V} identified in Section VI-B were compared to those generated offline by Dense Dijkstra that had access

TABLE II: LQMT Motion Primitives Time Trials.

Map	N	Planning time (ms)		Execution time (s)	
		Dense	STITCHER	Dense	STITCHER
Perlin Noise	4	7.95×10^4	1.75	3.30	3.66
	6	3.95×10^5	5.14	4.96	5.49
	8	7.32×10^5	10.33	8.16	8.73
Willow Garage	4	3.64×10^4	3.76	4.381	4.43
	6	3.34×10^5	10.00	5.694	6.14
	8	4.33×10^5	11.38	7.316	8.92

TABLE III: Minimum-Time Motion Primitives Time Trials.

Map	N	Planning time (ms)		Execution time (s)	
		Dense	STITCHER	Dense	STITCHER
Perlin Noise	4	4.29×10^7	6.41	2.51	2.75
	6	2.73×10^8	74.21	4.09	4.15
	8	2.86×10^8	191.21	7.05	7.18
Willow Garage	4	3.35×10^7	15.16	3.69	3.70
	6	1.49×10^8	111.06	4.92	5.05
	8	2.19×10^8	518.66	6.30	6.51

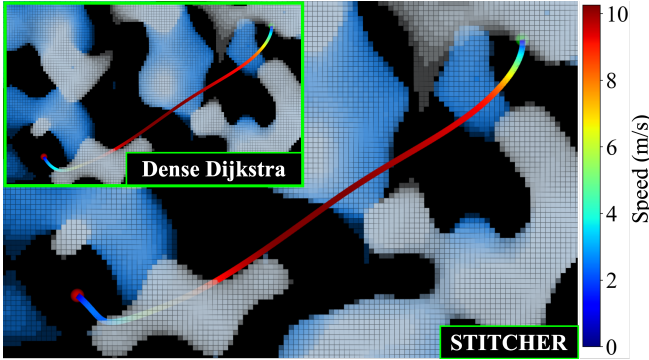


Fig. 8: Final trajectory computed by STITCHER with LQMT motion primitives through a pointcloud map of perlin noise. The Dense Dijkstra solution (computed offline) is shown in the inset for reference.

to a dense set of sampled velocities and/or accelerations. Table II shows the planning and execution times of STITCHER and the offline Dense Dijkstra solution using LQMT motion primitives. The trajectories generated by STITCHER typically have a longer execution time, within 10% of the dense solution, but has planning times that are four order of magnitude (10,000x) faster than the offline Dense Dijkstra planner across all tests. The substantial reduction in computation time with minimal impact on trajectory quality is a direct result of the proposed planning framework and innovative algorithmic elements of the proposed approach. Furthermore, similar trends are seen in Table III when using minimum-time motion primitives. On average STITCHER was within 3.2% of the dense solution in execution time, with a planning speed-up of over seven orders of magnitude (10,000,000x) for all tests. Note the increase in planning time with minimum-time motion primitives is expected as generating these primitives entails checking several cases [25]. Fig. 8 shows the trajectories generated by STITCHER and Dense Dijkstra in the perlin noise environment and the two trajectories are qualitatively indiscernible.

D. Heuristic Benchmarking

The quality of the heuristic used to guide STITCHER can be quantified by comparing the number of edges, i.e., motion primitives, generated by STITCHER to Dense Dijkstra. The

TABLE IV: Heuristic Evaluation for Edges Generated.

Map	N	Total Edges	Edges Generated		% Red.
			Dijkstra	STITCHER	
Perlin Noise	4	1023	769	558	27
	6	2945	2659	1767	34
	8	4867	4710	3401	28
Willow Garage	4	1023	580	567	2
	6	2945	1734	1385	20
	8	4867	3361	2563	24

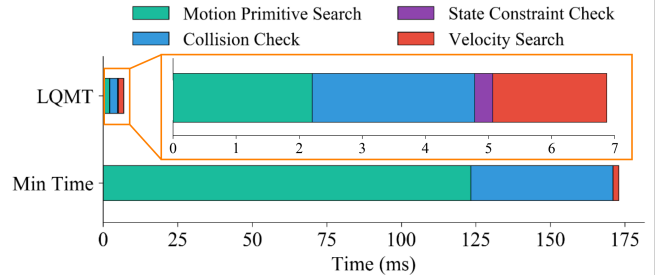


Fig. 9: The average contribution of different path planning components.

number of edges created is a better evaluation metric than nodes explored because motion primitive generation and evaluation is the main source of computation time. Table IV shows the number of edges created for STITCHER and Dense Dijkstra using LQMT motion primitives. The velocity magnitude and direction sets were kept constant across both planners with $|\mathcal{V}_m| = 11$ and $|\mathcal{V}_d| = 3$. STITCHER creates 30% fewer edges compared to Dense Dijkstra in the perlin noise environment whereas the percent reduction is 15.3% in the Willow Garage environment. The reduced effectiveness of the heuristic in the latter test case was attributed to having more tight corridors so more motion primitives were in collision (see, e.g., Fig. 2 top). This shows the heuristic is effective, but its performance does depend on the environment. Note that Dense Dijkstra does not generate the maximum possible number of edges because nodes become disconnected if motion primitives are found to be in collision or exceed state constraints.

E. Timing Analysis

Figure 9 shows the average time contribution of the different components that make up STITCHER. As expected, the minimum time motion primitive graph search and collision checking constitute more of the planning time compared to that of LQMT motion primitives due to the larger graph \mathcal{G}_{mp} accounting for terminal accelerations and the increased computation time required to generate motion primitives with several solution cases [25]. Checking for state constraints was found to be efficient, taking an average of 0.3 ms for LQMT motion primitives; minimum-time motion primitives inherently satisfy the constraints as part of their formulation. Lastly, the velocity search takes about 2 ms for both primitive classes indicating this is an effective method for computing an admissible heuristic for the motion primitive search.

F. Comparison with State-of-the-Art

Table V compares our LQMT STITCHER planner to two state-of-the-art algorithms: GCOPTER [5] and FASTER [9].

TABLE V: State-of-the-Art Comparison with LQMT Trajectories.

Map	N	Planning time (ms)			Execution time (s)		
		[9]	[5]	Ours	[9]	[5]	Ours
Perlin Noise	4	108	16.13	1.75	2.98	4.13	3.66
	6	187	50.52	5.14	4.42	4.70	5.49
	8	891	80.60	10.33	7.62	8.36	8.73
Willow Garage	4	262	12.30	3.76	4.39	5.45	4.43
	6	3527	32.95	10.00	7.07	8.12	6.14
	8	4524	94.24	11.38	8.75	FAILED	8.92

GCOPTER performs an online optimization by incorporating state constraints into the cost functional and running a quasi-newton method, while FASTER solves a mixed integer quadratic program online. Both algorithms rely on a sparse geometric path for safe corridor formation, but do not enforce final trajectories to pass through waypoints. STITCHER's planning times are faster than those measured for FASTER and GCOPTER for every test, and are up to 10x faster than GCOPTER and 400x faster than FASTER. In some cases GCOPTER and FASTER achieved lower execution times. This can be attributed to their ability to treat waypoints as soft constraints, i.e., the trajectory is only required to pass nearby a waypoint rather than through it. It is important to note the computation times for the motion primitive search planner [16] were omitted from Table II because planning times exceeded several seconds.

VII. CONCLUSIONS

In this work, we presented STITCHER, a motion primitive search planning algorithm that utilizes a novel three-stage planning architecture to design trajectories in real-time over long distances. We proved the search graph is finite, and the proposed search heuristic is admissible, so STITCHER is guaranteed to i) have *a priori* bounded time and memory complexity and ii) generate optimal trajectories with respect to the sampled set of states. Additionally, a new collision checking procedure was proposed to improve computational efficiency without artificially restricting the trajectory to pass through known free-space regions. Our extensive simulation study showed the trade-off in terms of path quality and computation time for different sampled velocity sets, the effectiveness of the proposed heuristic, and the average computation times of the components that make up STITCHER. Additionally, it was shown STITCHER consistently generates trajectories faster than two state-of-the-art optimization-based planners, with improvements ranging from one to two orders of magnitude. Future work includes developing a receding horizon implementation for navigating unknown environments, an extension for multi-agent coordination, the use of imitation learning to improve search efficiency, learning motion primitives for more general optimal control problems, and hardware experiments.

Acknowledgments Grace Kwak for data processing.

REFERENCES

[1] D. Mellinger and V. Kumar, "Minimum snap trajectory generation and control for quadrotors," in *IEEE Int. Conf. Robot. Autom.*, 2011, pp. 2520–2525.

[2] C. Richter, A. Bry, and N. Roy, "Polynomial trajectory planning for aggressive quadrotor flight in dense indoor environments," in *Int. Symp. Robot. Res.*, 2016, pp. 649–666.

[3] H. Oleynikova *et al.*, "Continuous-time trajectory optimization for online uav replanning," in *IEEE/RSJ Int. Conf. Intell. Robots Syst.*, 2016, pp. 5332–5339.

[4] B. Zhou, J. Pan, F. Gao, and S. Shen, "Raptor: Robust and perception-aware trajectory replanning for quadrotor fast flight," *IEEE Trans. Robot.*, vol. 37, no. 6, pp. 1992–2009, Dec. 2021.

[5] Z. Wang, X. Zhou, C. Xu, and F. Gao, "Geometrically constrained trajectory optimization for multicopters," *IEEE Trans. Robot.*, vol. 38, no. 5, pp. 3259–3278, May 2022.

[6] Y. Y. Ren *et al.*, "Bubble planner: Planning high-speed smooth quadrotor trajectories using receding corridors," in *IEEE/RSJ Int. Conf. Intell. Robots Syst.*, 2022, pp. 6332–6339.

[7] R. Deits and R. Tedrake, "Computing large convex regions of obstacle-free space through semidefinite programming," in *Algorithmic Foundations of Robotics*. Springer, 2015, pp. 109–124.

[8] —, "Efficient mixed-integer planning for uavs in cluttered environments," in *IEEE Int. Conf. Robot. Autom.*, 2015, pp. 42–49.

[9] J. Tordesillas, B. T. Lopez, M. Everett, and J. P. How, "FASTER: Fast and safe trajectory planner for navigation in unknown environments," *IEEE Trans. Robot.*, vol. 38, no. 2, pp. 922–938, Apr. 2022.

[10] T. Marcucci, M. Petersen, D. von Wrangel, and R. Tedrake, "Motion planning around obstacles with convex optimization," *Sci. Robot.*, vol. 8, no. 84, Nov. 2023.

[11] M. W. Mueller, M. Hehn, and R. D'Andrea, "A computationally efficient motion primitive for quadcopter trajectory generation," *IEEE Trans. Robot.*, vol. 31, no. 6, pp. 1294–1310, Dec. 2015.

[12] P. Florence, J. Carter, and R. Tedrake, "Integrated perception and control at high speed: Evaluating collision avoidance maneuvers without maps," in *Algorithmic Foundations of Robotics*. Springer, 2016, pp. 304–319.

[13] B. T. Lopez and J. P. How, "Aggressive 3-d collision avoidance for high-speed navigation," in *IEEE Int. Conf. Robot. Autom.*, 2017, pp. 5759–5765.

[14] M. Ryll, J. Ware, J. Carter, and N. Roy, "Efficient trajectory planning for high speed flight in unknown environments," in *IEEE Int. Conf. Robot. Autom.*, 2019, pp. 732–738.

[15] S. Liu, N. Atanasov, K. Mohta, and V. Kumar, "Search-based motion planning for quadrotors using linear quadratic minimum time control," in *2017 IEEE/RSJ international conference on intelligent robots and systems (IROS)*. IEEE, 2017, pp. 2872–2879.

[16] S. Liu, K. Mohta, N. Atanasov, and V. Kumar, "Search-based motion planning for aggressive flight in SE(3)," *IEEE Robot. Autom. Lett.*, vol. 3, no. 3, pp. 2439–2446, July 2018.

[17] B. Zhou, F. Gao, L. Wang, C. Liu, and S. Shen, "Robust and efficient quadrotor trajectory generation for fast autonomous flight," *IEEE Robot. Autom. Lett.*, vol. 4, no. 4, pp. 3529–3536, Oct. 2019.

[18] P. Foehn *et al.*, "Alphapilot: Autonomous drone racing," *Auton. Robots*, vol. 46, no. 1, pp. 307–320, Oct. 2021.

[19] S. Liu *et al.*, "Planning dynamically feasible trajectories for quadrotors using safe flight corridors in 3-d complex environments," *IEEE Robot. Autom. Lett.*, vol. 2, no. 3, pp. 1688–1695, July 2017.

[20] M. Hehn and R. D'Andrea, "Quadcopter trajectory generation and control," *IFAC Proc. Vol.*, vol. 44, no. 1, pp. 1485–1491, Jan. 2011.

[21] B. T. Lopez and J. P. How, "Aggressive collision avoidance with limited field-of-view sensing," in *IEEE/RSJ Int. Conf. Intell. Robots Syst.*, 2017, pp. 1358–1365.

[22] D. Dolgov, S. Thrun, and M. Montemerlo, "Path planning for autonomous vehicles in unknown semi-structured environments," *Int. J. Robot. Res.*, vol. 29, no. 5, pp. 485–501, Jan. 2010.

[23] M. Pivtoraiko and A. Kelly, "Kinodynamic motion planning with state lattice motion primitives," in *IEEE/RSJ Int. Conf. Intell. Robots Syst.*, 2011, pp. 2172–2179.

[24] A. Romero, S. Sun, P. Foehn, and D. Scaramuzza, "Model predictive contouring control for time-optimal quadrotor flight," *IEEE Trans. Robot.*, vol. 38, no. 6, pp. 3340–3356, Dec. 2022.

[25] L. Berscheid and T. Kröger, "Jerk-limited real-time trajectory generation with arbitrary target states," in *Robot.: Sci. Syst.*, 2021.

[26] S. J. Russell and P. Norvig, *Artificial intelligence: a modern approach*. Pearson, 2016.

[27] D. E. Kirk, *Optimal control theory: an introduction*. Courier Corporation, 2004.